Electronic Supplementary Information

Confined semiconducting polymers with boosted NIR light- triggered H_2O_2 production for hypoxia-tolerant persistent photodynamic therapy

Feng Lu,[a] Lili Li,[a] Meng Zhang,[a] Chengwu Yu,[a] Yonghui Pan,[a] Fangfang Cheng,[b] Wenbo Hu,[c] Xiaomei Lu,[d,e] Qi Wang*[a] and Quli Fan*[a]

[a]State Key Laboratory of Organic Electronics and Information Displays, Jiangsu Key Laboratory for Biosensors, Institute of Advanced Materials (IAM), Nanjing University of Posts & Telecommunications, Nanjing 210023, China.

[b]School of Pharmacy, Nanjing University of Chinese Medicine, Nanjing 210023, China

[c]Institute of Flexible Electronics (IFE), Northwestern Polytechnical University, Xi'an 710072, China

[d]Institute of Advanced Materials (IAM) & School of Flexible Electronics (Future Technologies), Nanjing Tech University, Nanjing, 211816, China

[e]Zhengzhou lnstitute of Biomedical Engineering and Technology, Zhengzhou, 450001, China

1. Materials and instruments

Materials: (4,4-bis(2-ethylhexyl)-4*H*-cyclopenta[1,2-*b*:5,4-*b*']dithiophene-2,6-diyl)bis(trimethylstannane) (**1**) was obtained from JiangSu GR-Chem Biotech Co., Ltd. 4,7-dibromo-2,1,3-benzothiadiazole (**2**) and doxorubicin hydrochloride (DOX) were supplied by Energy Chemical. Poly[2,6-(4,4-bis-(2-ethylhexyl)-4*H*-cyclopenta[2,1-*b*;3,4-*b'*]dithiophene)-*alt*-4,7(2,1,3-benzothiadiazole)] (PCPDTBT) was prepared according to the literature.[1] NaOH, tetraethyl orthosilicate (TEOS), PEG-*b*-PPG-*b*-PEG (F127), hexadecyltrimethylammonium bromide (CTAB), and 1,3-diphenylisobenzofuran (DPBF) were purchased from Sigma-Aldrich. 3,3',5,5'-tetramethylbenzidine (TMB) and ethyl acetate were obtained from TCI (Shanghai) Development Co., Ltd. 2-[Methoxy(polyethyleneoxy)$_{9\text{-}12}$propyl] trimethoxysilane (PEG 500) were obtained from J&K Scientific Ltd. Peroxidase from horseradish (HRP) and mPEG-silane 5K (PEG 5000) were provided by Shanghai Aladdin Biochemical Technology Co., Ltd. Doxorubicin hydrochloride (DOX) were supplied by Energy Chemical. 3-(4,5-dimethyl-2-thiazolyl)-2,5-diphenyl-2-tetrazolium bromide (MTT) and 2,7-Dichlorodihydrofluorescein diacetate (DCFH-DA) were obtained from KeyGen Biotech. Co., Ltd. Dihydroethidium (DHE), ethanol, 1,10-Phenanthroline, and $FeCl_2$•$4H_2O$ were purchased from Shanghai Macklin Biochemical Co., Ltd. Singlet oxygen sensor green (SOSG) was provided by Thermo Fisher Scientific. ROS-ID™ hypoxia/oxidative stress detection kit was purchased from Enzo Life Sciences Inc. Aminophenyl fluorescein (APF) and ROSGreen™ H_2O_2 Probe were obtained from Shanghai Maokang Biotechnology Co., Ltd. Superoxide Anion Content Assay Kit was purchased from Beijing Boxbio Science & Technology Co., Ltd. Amplex Red, GSH and GSSG Assay Kit, and Cellular Glutathione Peroxidase Assay Kit were obtained from Shanghai Beyotime Biotechnology. Malondialdehyde (MDA) Content Assay Kit was purchased from Sangon Biotech (Shanghai) Co., Ltd. Cancer cells and culture media were all obtained from KeyGen Biotech. Co., Ltd.

Characterization: Transmission electron microscopy (TEM) images were captured by HT7700 transmission electron microscope (HITACHI) at an acceleration voltage of 100 kV. The absorption spectra were obtained with a UV-3600 UV-vis-NIR spectrophotometer (Shimadzu). The fluorescence spectra in the NIR-II region were acquired with a Horiba Fluorolog 3 spectrophotometer (Horiba JobinYvon). The fluorescence spectra (400-850 nm) and fluorescence decay curves were measured with a FLS 980 fluorescence spectrometer (Edinburgh). High resolution transmission

electron microscopy (HRTEM) image and elemental mapping were obtained with FEI Talos 200x high resolution transmission electron microscope (Thermo Fisher). The femtosecond transient absorption (fs-TA) spectra were obtained on a lab-built experimental setup (Helios, Ultrafast Systems) with a temporal resolution of ca. 170 fs. An amplified Ti:sapphire laser system to produce a fundamental 800 nm output with a pulse width of 120 fs and a 1 kHz repetition rate (Solstice Ace, Spectra-Physics). This laser system provides an average power of 7 W, which was divided into two beams (7:3) for pump and probe, respectively. The pump beam with a wavelength of 660 nm was generated through an optical parametric amplifier (TOPAS, Light Conversion). The other beam was focused in a 3 mm Saphire plate and filtered by a short pass filter (800 nm) to cut off the fundamental 800 nm laser pulse and produce a white light continuum, which was used as a probe pulse ranging from 420 to 850 nm. The zeta potential and hydrodynamic diameter were measured on a Particle Size Analyzer 90Plus (Brookhaven). Confocal laser scanning microscopy (CLSM) images were acquired using a LSM 880 NLO microscope (ZEISS). Fluorescence imaging in the NIR-II region was performed using a NIRvana 640 2D InGaAs FPA camera (Princeton Instruments) equipped with a 980 nm long-pass filter (semrock). An 808 nm laser with a power density of ~60 mW/cm^2 was used as excitation source.

2. Synthesis of PCPDTBT:

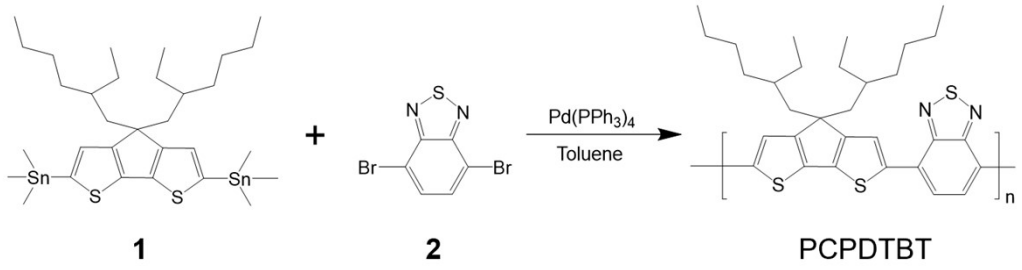

Scheme S1. Synthetic route of PCPDTBT.

Monomer **1** and **2** (0.1 mmol each) and $Pd(PPh_3)_4$ (10 mg) were added to a 50 mL Schlenk flask. The reaction tube was subjected to 3 pump/purge cycles with nitrogen, and then injected with 8 mL of anhydrous toluene via syringe. The reaction was performed at 100 for 24 h. After cooling to the room temperature, the mixture was dripped into methanol under stirring, the precipitate was filtered and washed several times with methanol. Black colored solid was obtained after drying under reduced

pressure. Mw =9568 Da, PDI =1.35. ^{1}H NMR (400 MHz, $CDCl_3$, 298 K) δ(ppm): 8.2-8.0 (br m, 2H), 8.0-7.8 (br m, 2H), 2.2-1.9 (br m, 4H), 1.1-0.6 (br m, 30H).

3. Synthesis of SP@mSiO$_2$-PEG: 50 mg CTAB was first dissolved in 2.5 mL water at 50 ℃, then 0.4 mL of PCPDTBT (1 mg/mL) in chloroform was dropwise added to the CTAB solution under vigorous stirring. After the microemulsion was formed under sonication, the chloroform was evaporated at 60 ℃ and then the solution was further heated at 70 ℃ for 10 min. The CTAB stabilized PCPDTBT solution was then mixed with 22.5 mL water at 70 ℃ and stirred for 10 min. 125 μL TEOS, 0.5 mL ethyl acetate and 188 μL NaOH (2M) were added to the above solution quickly. After 40 min, 200 mg of mPEG-silane 5K was added to PEGylated the mesoporous silica nanoparticles. 50 μL PEG 500 was injected 1 h later and stirred for 2 h to further PEGylated the nanoparticles. Finally, the obtained SP@mSiO$_2$-PEG was purified by ultrafiltration tube (30 K). The CTAB template can be removed by stirring the nanoparticles in 10 mg/mL NH_4NO_3 ethanol solution at 50 ℃ together with 50 μL PEG500.

4. Synthesis of SP@F127: 20 mg F127 was first mixed with 1 mL THF solution containing 0.25 mg of PCPDTBT, then rapidly injected to 9 mL water under sonication. After 3 min of sonication, the solution was stirred on at 50 under nitrogen atmosphere to remove the THF. The nanoparticles were obtained after purification with ultrafiltration tube (30 K).

5. Synthesis of SP@mSiO$_2$-PEG/FeDOX: Fe^{2+} ions were loaded by mixing 200 uL of $FeCl_2$•$4H_2O$ aqueous solution (1 mg/mL) with 2 mg of SP@mSiO$_2$-PEG in 4 mL water. After 3h stirring at room temperature and ultrafiltration, SP@mSiO$_2$-PEG/Fe was obtained. Then, 0.4 mL of DOX solution (1 mg/mL) was added to the above solution and stirred overnight in dark. The solution was washed twice with water by ultrafiltration to obtain SP@mSiO$_2$-PEG/FeDOX.

6. Drug loading capacity and release: The loading capacity of Fe^{2+} was evaluated by comparing the Fe^{2+} concentration before and after loading process, which was determined by 1,10-phenanthroline chelation method.[2] Similarly, the loading capacity of DOX was determined by comparing the change the absorbance of DOX before and after loading. In order to investigate the release behavior of Fe and DOX, the obtained SP@mSiO$_2$-PEG/FeDOX was added to 1.5 mL buffers with different pHs and stirred in the dark. At desired time intervals, the solution was centrifuged and 1 mL of supernatant was taken out for characterization, and 1 mL of fresh buffer was added

thereafter. The concentrations of DOX and Fe^{2+} in the supernatant were determined by absorption spectra and ICP-MS, respectively.

7. In vitro ROS detection: For singlet oxygen ($^1O_2$) detection, the obtained nanoparticles were diluted to an absorbance of ~0.3 at 730 nm. Then, 2.5 mL of diluted sample was mixed with 50 μL DBPF (1 mg/mL in ethanol), and irradiated with 730 nm laser with a power density of 80 mW/cm^2. The decay of the absorbance of DPBF at 417 nm was used to quantify the generation of $^1O_2$.

For hydroxyl radical (•OH) detection, the obtained nanoparticles were diluted with NaAc/HAc buffer (pH 4) to an absorbance of ~0.3 at 730 nm. Then, 2.5 mL diluted sample was mixed with 10 μL TMB (80 mM in DMSO), and then irradiated with 730 nm laser (80 mW/cm^2). The change of the absorbance at 656 nm was used to analyze the generation of •OH.

For hydrogen peroxide (H_2O_2) detection, the obtained nanoparticles were diluted with TAPS buffer (pH 8.2) containing HRP (10 U/mL) and Amplex Red (40 μM). The elevation of the absorbance at 572 nm was used to quantify the generation of H_2O_2 under 730 nm laser.[3]

8. Detection of ROS with EPR: 200 μL of the obtained nanoparticles (0.5 mg/mL) were mixed with 10 μL TEMP and 20 μL DMPO, respectively. And then exposed to 730 nm laser for 5 min to detect $^1O_2$ and •OH. The samples without laser irradiation and the spin-trapping agents with laser irradiation were examined as controls.

9. Intracellular ROS detection: 4T1 cells were seeded in a 3.5 cm confocal dish overnight, then replaced with fresh culture medium together with 15 μL 20 μg/mL SP@mSiO_2-PEG and incubated in dark for 5 h. The ROS probes were added and incubated for another 30 min. After wash, the cells were exposed to a 730 nm laser (230 mW/cm^2) and immediately subjected to a CLSM to visualize various ROS species. The hypoxic environment was mimicked with Mitsubishi™ AnaeroPack.[4] Total ROS, $^1O_2$, •OH, and H_2O_2 were detected with DCFH-DA, SOSF, APF, and ROSGreen respectively, the concentration of the probes were adjusted according to the product manual.

10. Determination of GSH and GSSG in cells: Cells with a density of 2×10^5 cells per well were cultured overnight, and then incubated with SP@mSiO_2-PEG or SP@mSiO_2-PEG/FeDOX nanoparticles (40 μg/mL) for 5 h and exposed to 730 nm laser for 10 min. After wash, the cells were collected and used for GSH and GSSG assay according to

the manufacturer's instructions. The cells treated without laser irradiation and without nanoparticles were also analyzed for comparison.

11. Relative GPX4 activity determination: Cells were seeded in 6-well plate and cultured overnight. When the cell confluence reached ~70%, SP@mSiO_2-PEG or SP@mSiO_2-PEG/FeDOX nanoparticles (40 μg/mL) were added and incubated for 5 h before irradiation with 730 nm laser. Then, the cells were collected for GPX4 activity assay using Cellular Glutathione Peroxidase Assay Kit with DTNB according to the manufacturer's instructions.

12. Intracellular MDA assay: Cancer cells were first seeded in a culture dish, SP@mSiO_2-PEG or SP@mSiO_2-PEG/FeDOX nanoparticles (40 μg/mL) was added when the cells covered ~90% of the dish. After 5 h, the cells were irradiated with 730 nm laser for 10 min, and then the cells were collected for MDA assay with lipid peroxidation MDA Assay Kit according to the manufacturer's protocol.

13. In vitro cytotoxicity: Cells were seeded in 96-well plates with a density of 5×10^3 cells per well and cultured overnight. Then, the cells were incubated with SP@mSiO_2-PEG and SP@mSiO_2-PEG/FeDOX nanoparticles with different concentrations for 20 h. The cells were irradiated with 730 nm with a power density of 230 mW/cm^2 and further cultured for 4 h. Standard MTT assay was then carried out to detect the cytotoxicity of nanoparticles. The cell viabilities of the cells treated without laser irradiation and without nanoparticles were determined for comparison. The hypoxic environment was created with Mitsubishi™ AnaeroPack 2 h before laser irradiation.

14. Animal model: All mice was obtained from Jiangsu KeyGEN BioTECH Corp., Ltd and used according to the guidelines of the Laboratory Animal Center of Jiangsu KeyGEN BioTECH Corp., Ltd. The 4T1 tumor models were achieved by subcutaneous injection of 4T1 tumor cells in the right armpit of the mice. When the tumor volume reached ~200 mm^3, the mice was used for in vivo imaging. For phototherapy, the tumor volume was grown to ~100 mm^3. The animal experiments were approved by the Animal Ethics Committee of the institution of Nanjing University of Chinese Medicine (202112A008).

15. In vivo NIR-II fluorescence imaging: The tumor-bearing mice was depilated and intravenous injected with the 150 μL of nanoparticles at a concentration of 1 mg/mL through the tail vein. The fluorescence images at different time points were captured with a NIRvana 640 InGaAs camera equipped with 980 nm long-pass filter. 808 nm

laser was adopted as the excitation source, and the power density was adjusted to ~60 mW/cm^2 on the animal surface. The images were processed and analyzed with the software ImageJ.

16. In vivo phototherapy: The tumor-bearing mice were randomly divided into five groups (n=4), and treated with different formulations: (i) saline, (ii) SP@mSiO$_2$-PEG, (iii) SP@mSiO$_2$-PEG/FeDOX, (iv) SP@mSiO$_2$-PEG + laser, and (v) SP@mSiO$_2$-PEG/FeDOX + laser. The nanoparticles (1 mg/mL, 150 μL) were intravenous injected, and laser irradiation was carried out at 48 h post-injection. The power density of the 730 nm laser was around 230 mW/cm^2 and the exposure time was 10 min.

17. Computational Methods: The alkyl chains of PCPDTBT was approximated as the methyl groups, and three CPDTBT units were used for the simulation. The equilibrium geometry of the ground state was obtained based on the density functional theory using the Gaussian 09 program at the B3LYP/6-31G(d) level of theory.[5]

18. Statistical analysis: For each experiment, data were reported as means ± standard deviation. *T*-test was performed for statistical analysis. *P*-value of < 0.05 was considered significant. *$p < 0.05$, **$p < 0.01$, ***$p < 0.001$.

Table S1. The advantages of semiconducting polymers for NIR-II imaging and PDT.

NIR-II imaging	Photodynamic therapy
High photostability	
Easy synthesis and scalability	
Good biocompatibility	
Tunable absorption/emission peak	Broad absorption spectrum
Large Stokes shift	Large extinction coefficient
Wide emission spectrum range	Efficient ROS generation

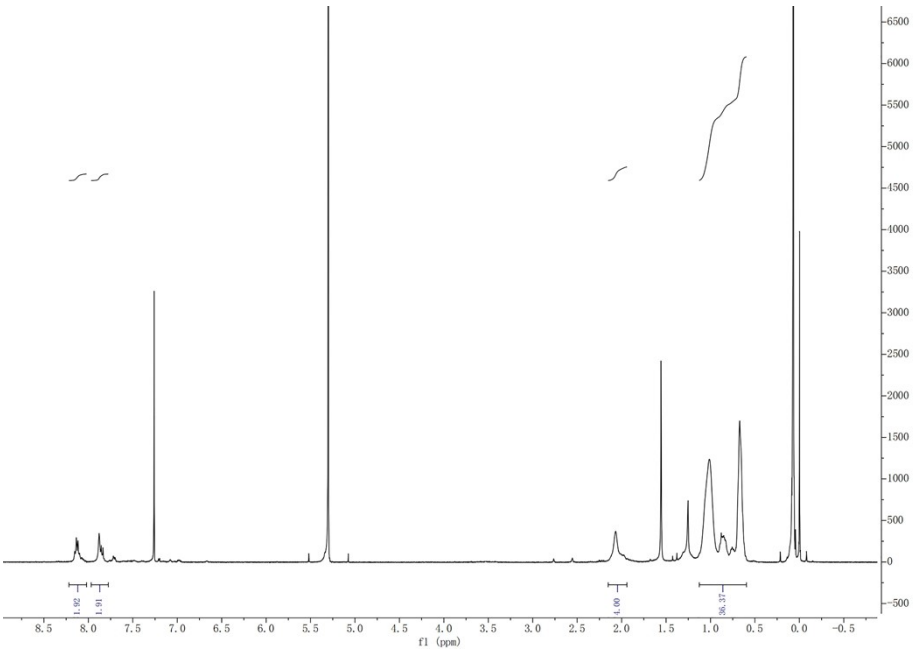

Figure S1. ^{1}H-NMR (400 MHz, $CDCl_3$) of synthesized PCPDTBT.

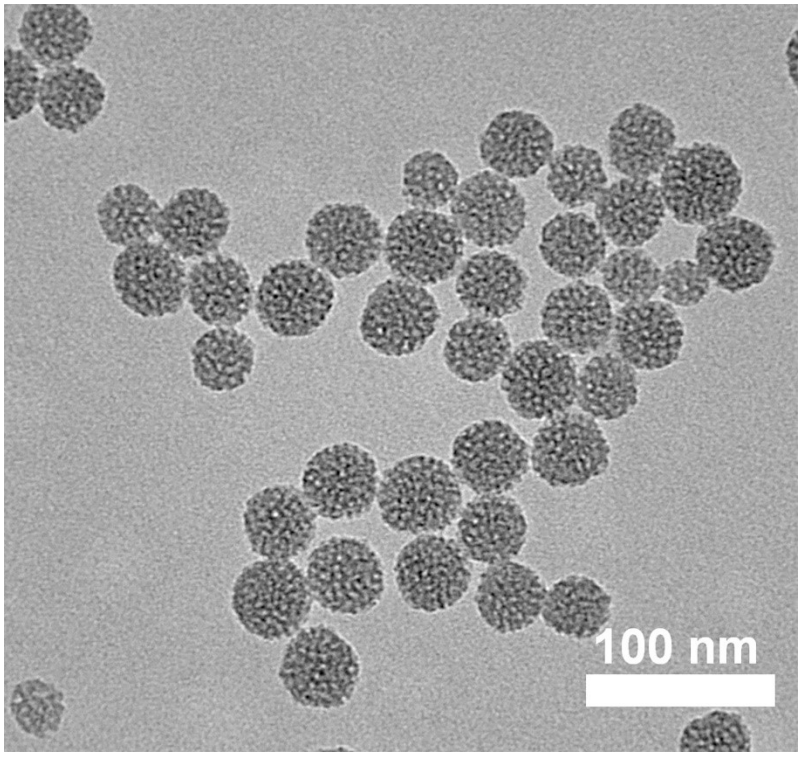

Figure S2. Enlarged TEM image of SP@mSiO_2-PEG.

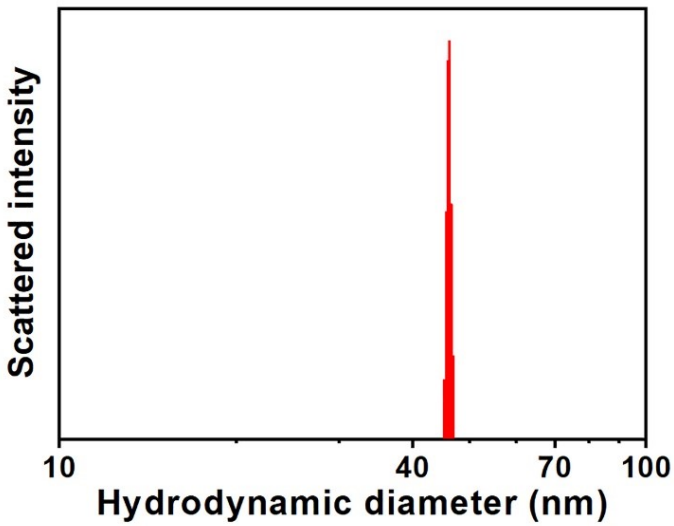

Figure S3. Hydrodynamic diameter of SP@F127.

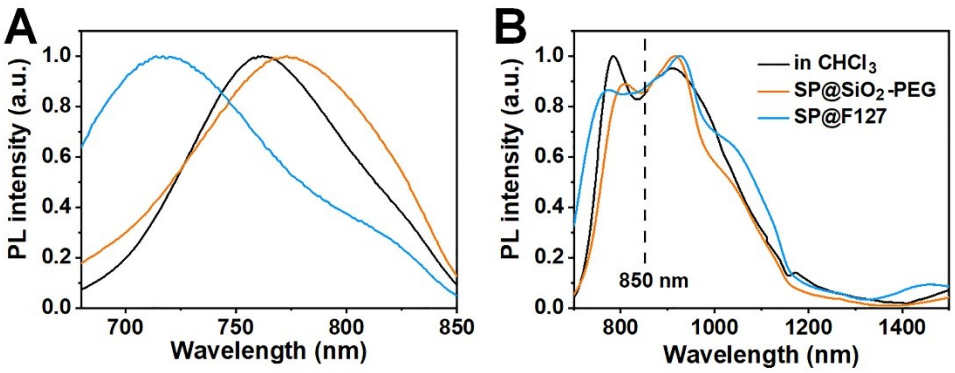

Figure S4. A) Normalized emission spectra acquired with a silicon-based detector. B) Normalized emission spectra of the data in Figure 1E.

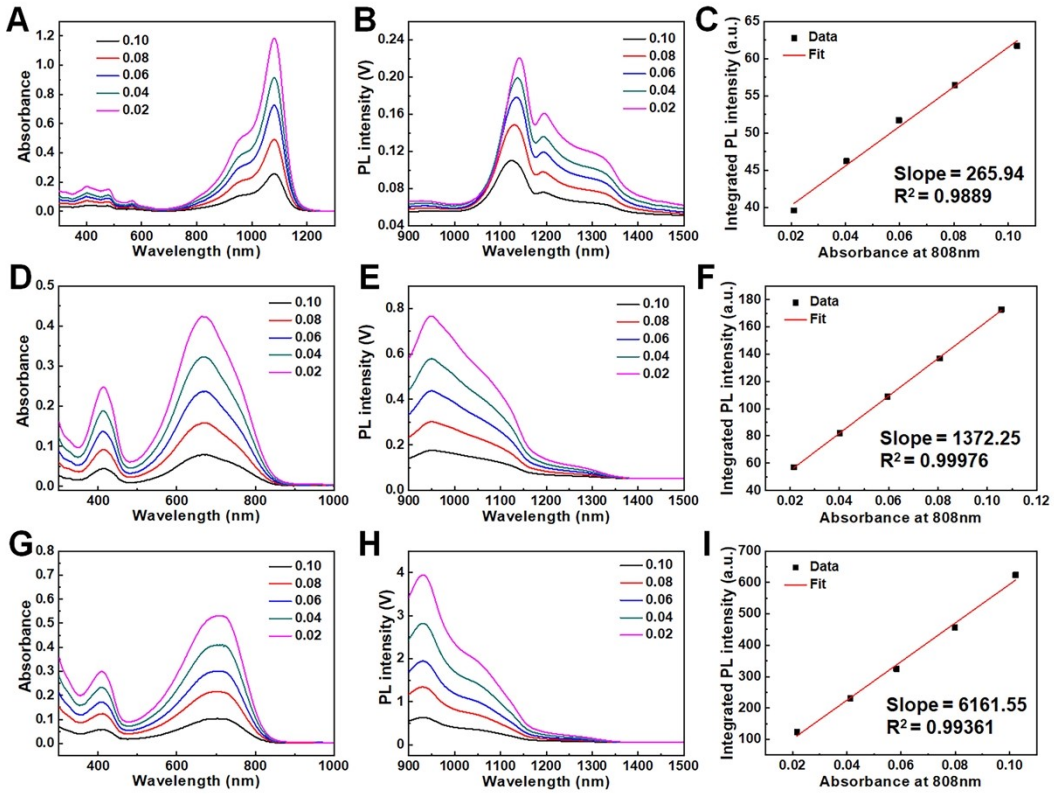

Figure S5. Absorption spectra of A) IR-26 reference solutions in 1,2-dichloroethane, D) SP@F127 in water, and G) SP@mSiO$_2$-PEG in water at different concentrations. Their absorbance at 808 were adjusted to ~0.02, ~0.04, ~0.06, ~0.08, ~0.10, respectively. Emission spectra of B) IR-26 reference solutions, E) SP@F127, and H) SP@mSiO$_2$-PEG under 808 nm excitation. The linear fitting of the integrated PL intensities (900-1500 nm) versus the absorbance values of C) IR-26, F) SP@F127, and I) SP@mSiO$_2$-PEG at 808 nm.

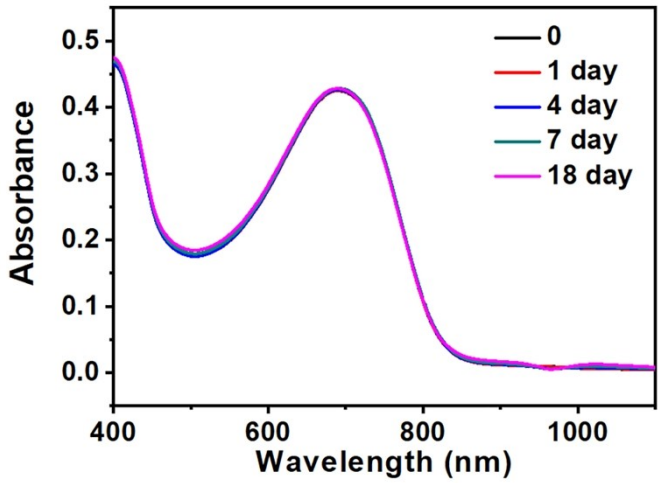

Figure S6. The absorption spectra of SP@mSiO$_2$-PEG stored for different period of time.

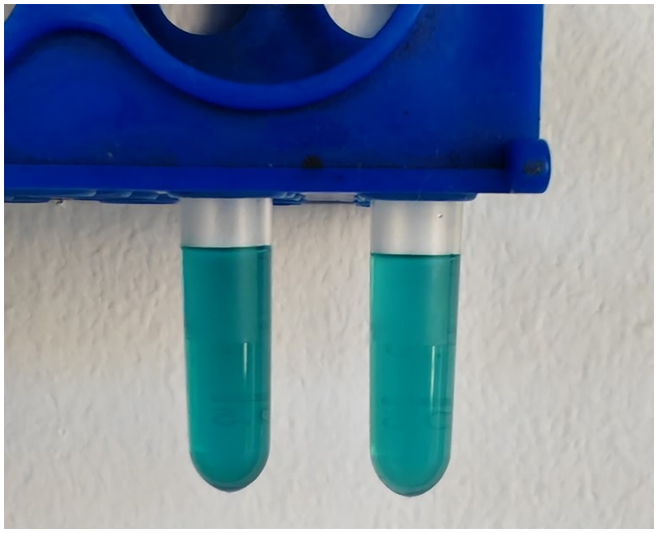

Figure S7. Photograph of some typical SP@mSiO$_2$-PEG samples prepared in August 2022.

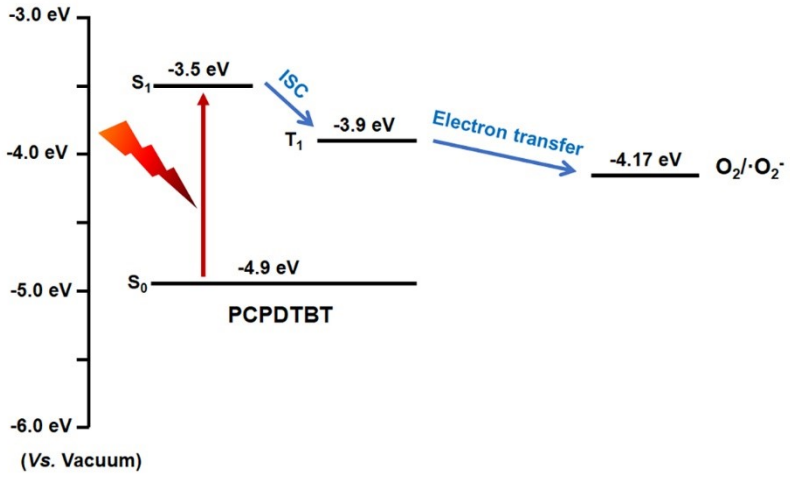

Figure S8. Proposed mechanism of type I PDT process with PCPDTBT under NIR laser irradiation.

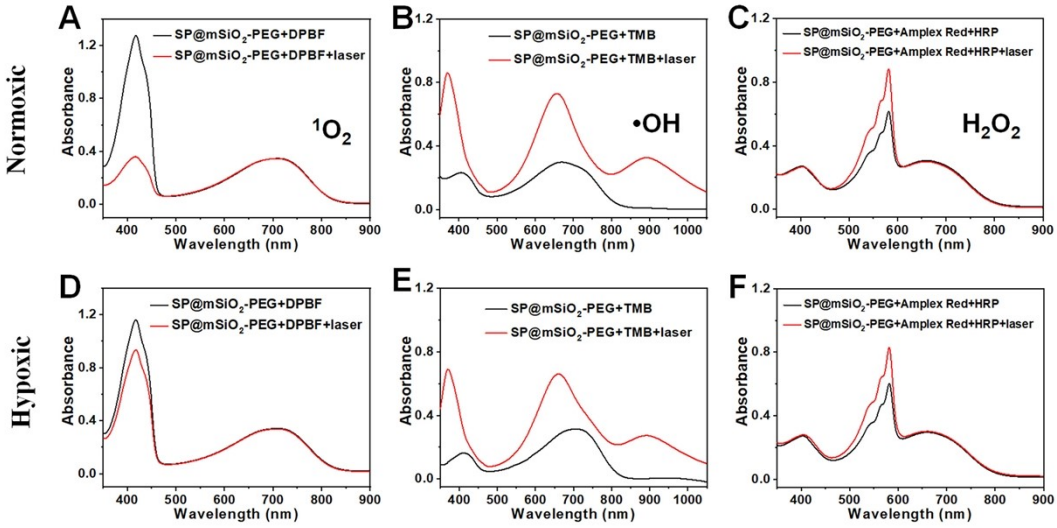

Figure S9. Photo-induced A) $^1O_2$, B) •OH, and C) H_2O_2 generation of SP@mSiO_2-PEG under normoxic condition. Photo-induced D) $^1O_2$, E) •OH, and F) H_2O_2 generation of SP@mSiO_2-PEG under hypoxic condition.

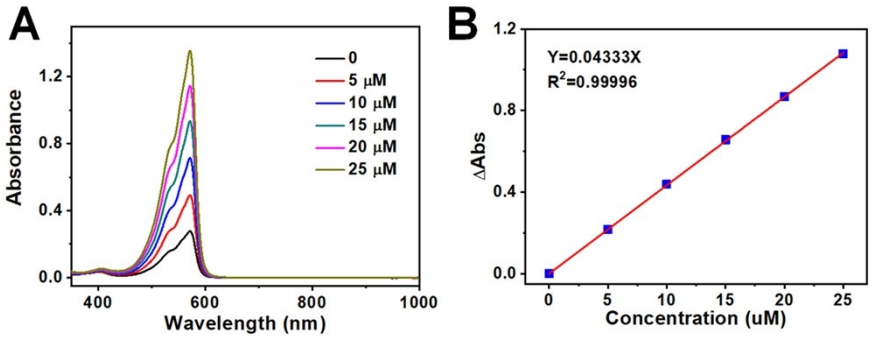

Figure S10. A) Absorption spectra of Amplex Red with different concentrations of H_2O_2, and B) the corresponding linear fitting curve. This curve was used for the calculation of H_2O_2 production of SP@mSiO_2-PEG in Figure 2K.

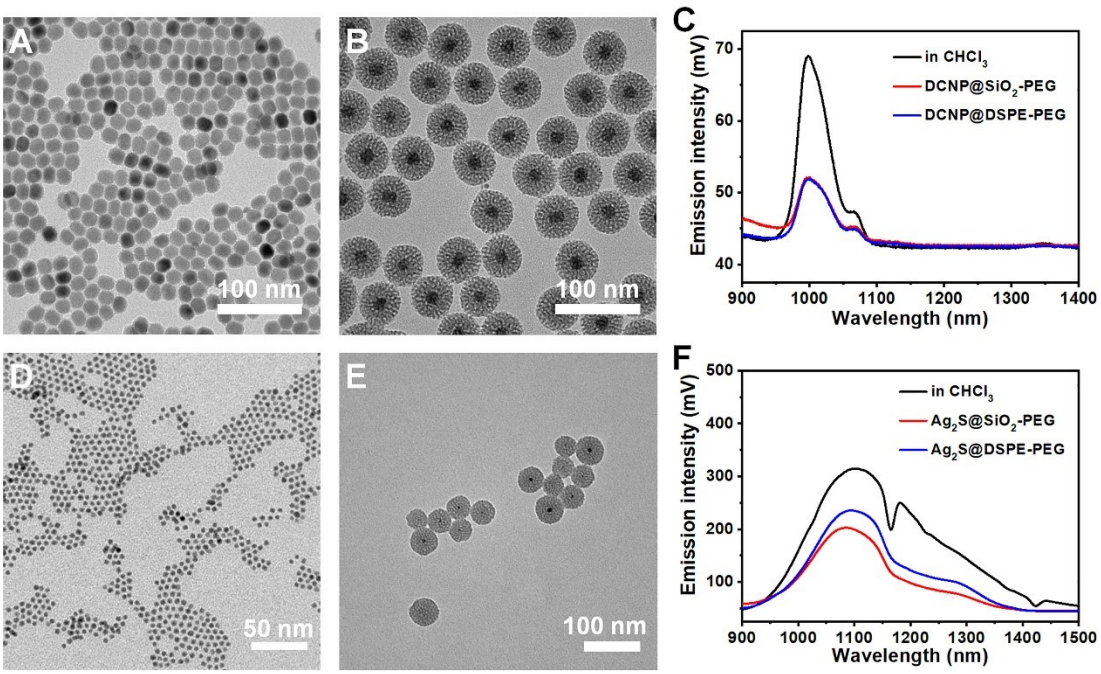

Figure S11. TEM image of A) $NaYF_4$:$Yb_{0.05}$,$Nd_{0.2}$@$NaYF_4$ (DCNP) and D) Ag_2S QDs. TEM image of B) DCNP@SiO_2-PEG and E) Ag_2S@SiO_2-PEG nanoparticles. Emission spectra of C) DCNP and F) Ag_2S QDs before and after surface modifications. DCNP[6], DCNP@SiO_2-PEG[7] and Ag_2S@SiO_2-PEG[8] were prepared according to the previous reports.

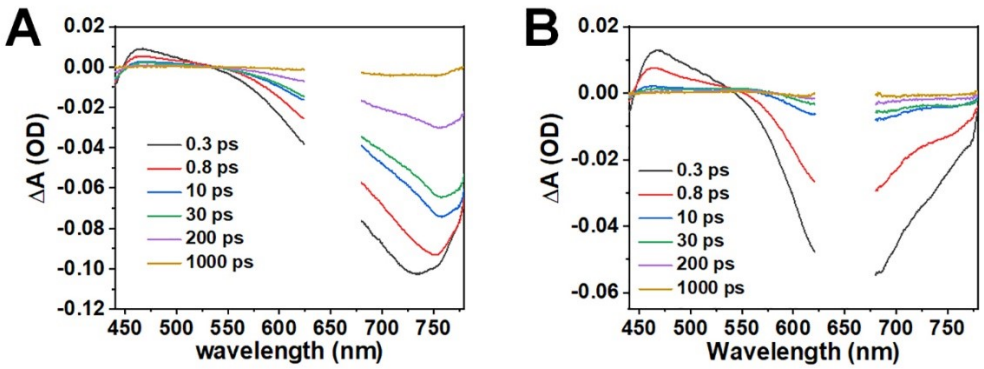

Figure S12. Representative fs-TA plots of A) SP@mSiO$_2$-PEG, and B) SP@F127 at different delay times.

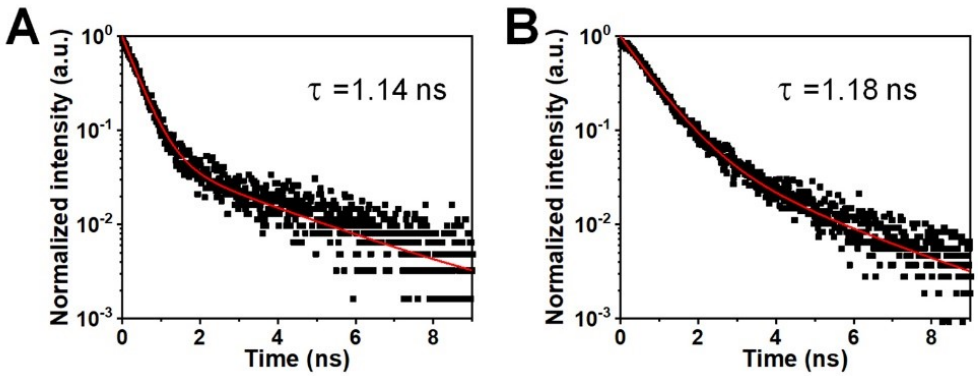

Figure S13. Fluorescence decay curves of A) SP@mSiO$_2$-PEG, and B) SP@F127 at 820 nm.

Table S2. Photophysical properties of the nanoparticles.

	SP@mSiO$_2$-PEG	SP@F127
PLQY$_{900\text{-}1500\ nm}$ (%)	9.872	2.198
PLQY$_{NIR\text{-}II}$ (%)	4.582	1.188
PLQY$_{total}$ [a] (%)	18.899	4.194
τ (ns)	1.14	1.18
K_f [b] (s^{-1})	1.66×10^8	3.55×10^7
$K_f+K_{nr}+K_{isc}$ [c] (s^{-1})	8.77×10^8	8.47×10^8

[a] The total photoluminescence quantum yield was calculated based on the emission spectra in Fig. 1E;
[b] K_f is the rate of fluorescence;
[c] K_{nr} is the sum of the rates of nonradiative decays; K_{isc} is the rate of intersystem crossing.

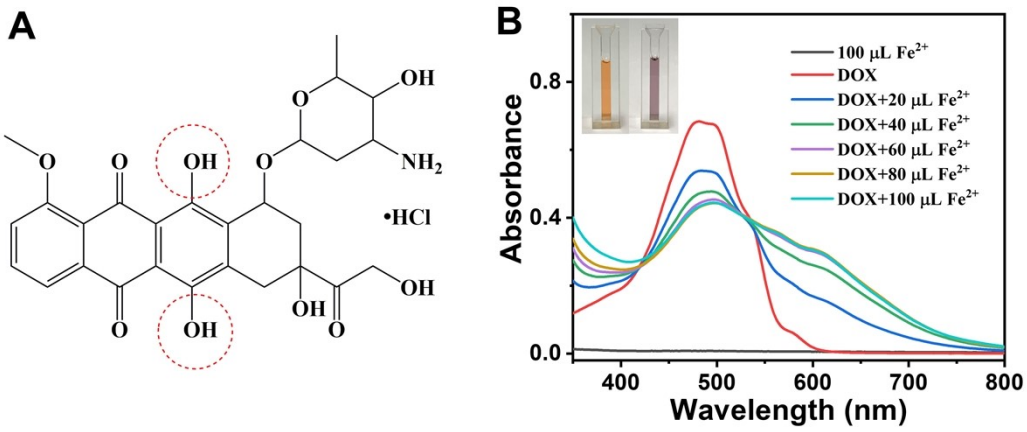

Figure S14. (A) Chemical structure of DOX. (B) The absorption spectra of DOX solution (94.8 μM, 3 mL) mixed with different volume of $FeCl_2$ solution (1 mM). The inset shows the photographs of DOX solution before and after mixing with Fe^{2+} ions.

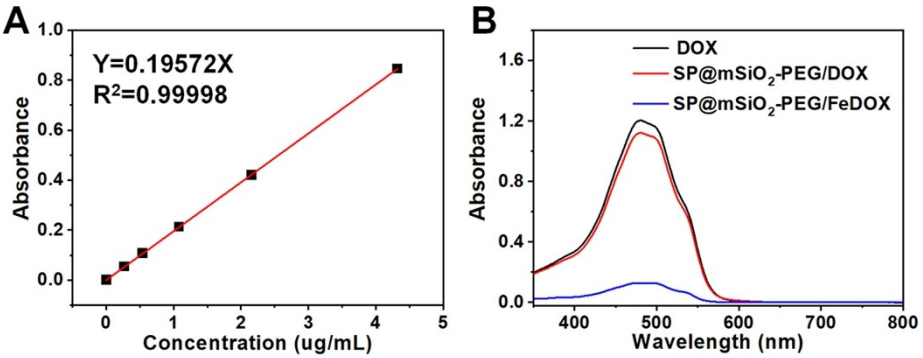

Figure S15. A) Calibration curve between the absorbance at 510 nm and the concentration of Fe^{2+} ions. B) Absorption spectra of DOX suspension before and after being loaded with SP@mSiO_2-PEG and SP@mSiO_2-PEG/Fe.

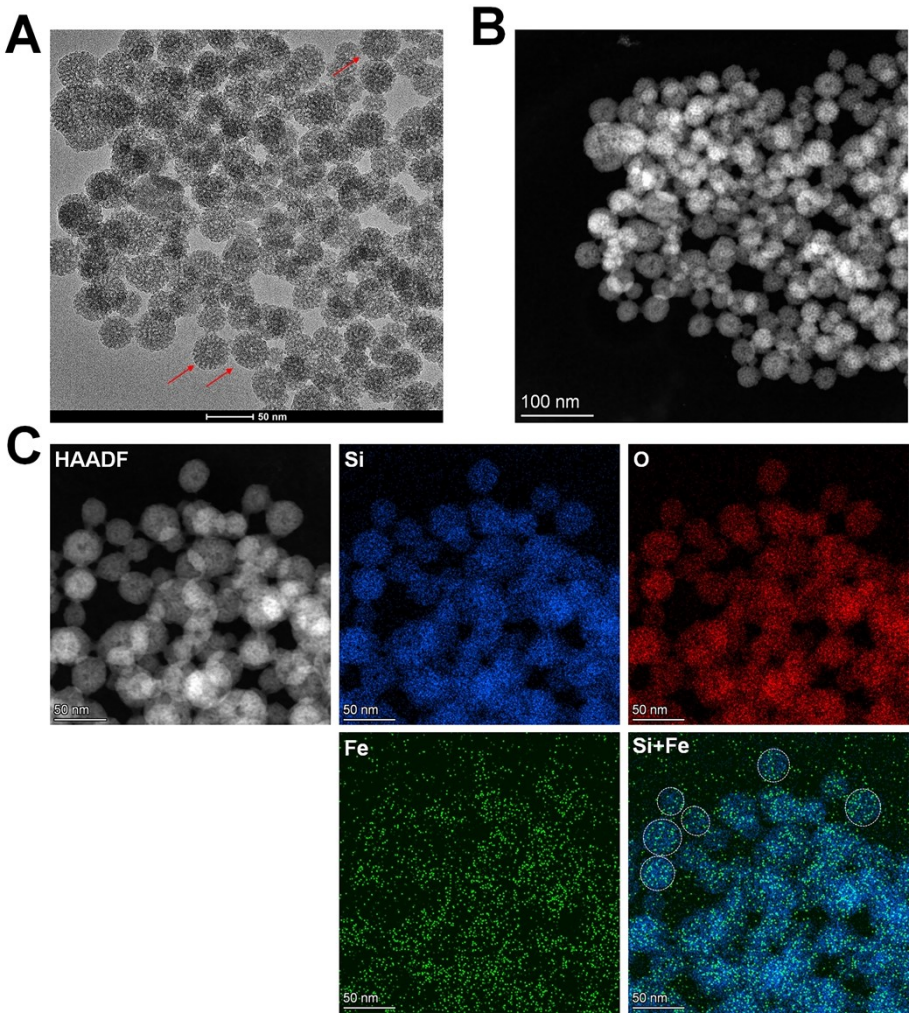

Figure S16. HRTEM image (A), HAADF-STEM image (B), and elemental mapping (C) of the obtained nanocomposites.

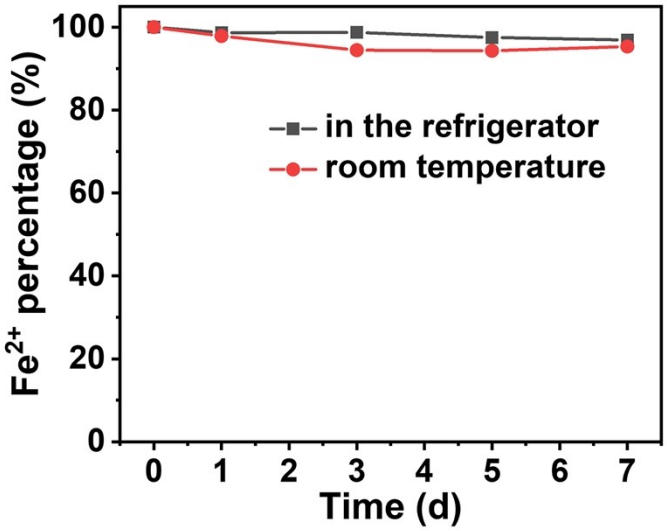

Figure S17. The percentage of Fe^{2+} remained in $FeCl_2$ solutions after being stored in the refrigerator and at room temperature. The concentration of Fe^{2+} was determined with 1.10-phenanthroline.

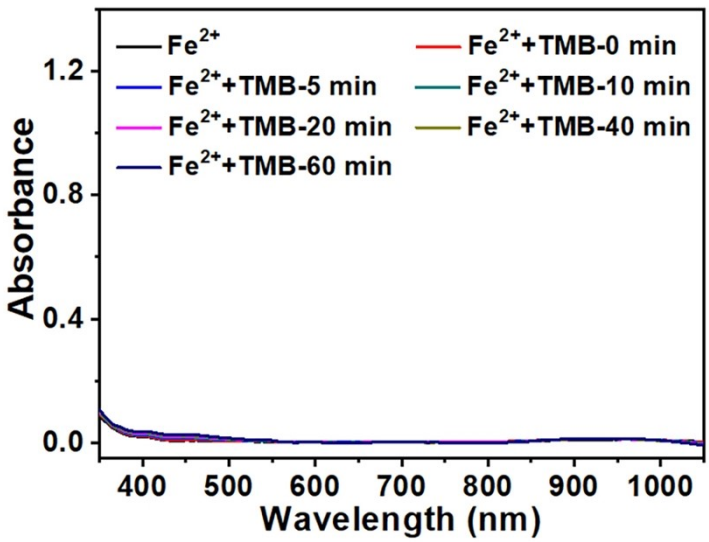

Figure S18. The evolution of the absorption spectra of Fe^{2+} ions after the addition of TMB for different times.

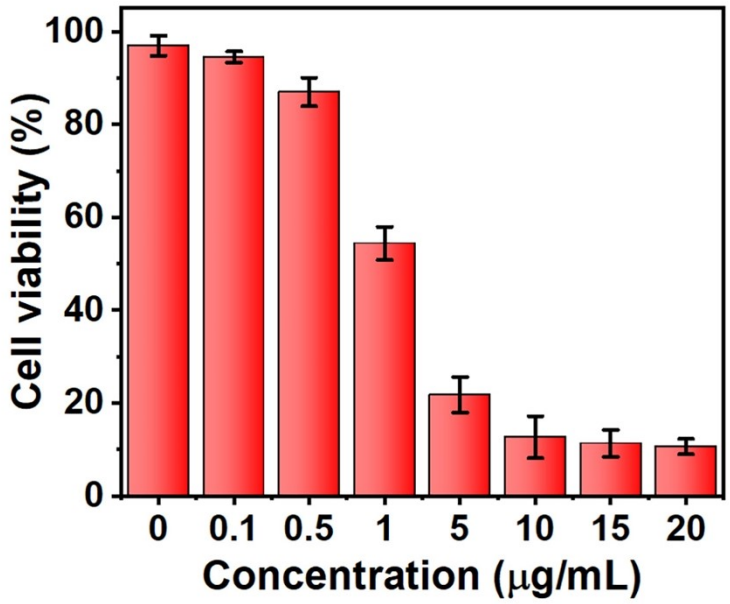

Figure S19. Cell viabilities of 4T1 cells after incubated with DOX at different concentrations.

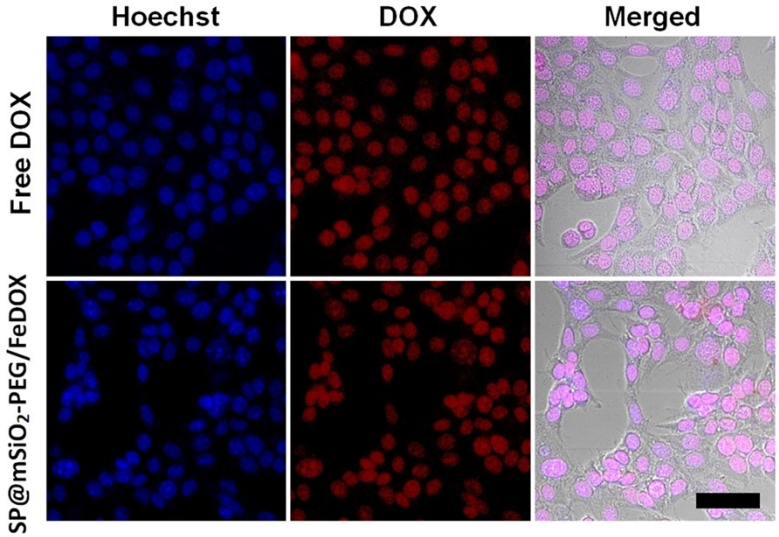

Figure S20. CLSM images of 4T1 cells incubated with free DOX and SP@$mSiO_2$-PEG/FeDOX nanoparticles for 12 h (DOX concentration: 8 μg/mL), which verified the nuclear targeting ability of DOX. The scale bar is 50 μm.

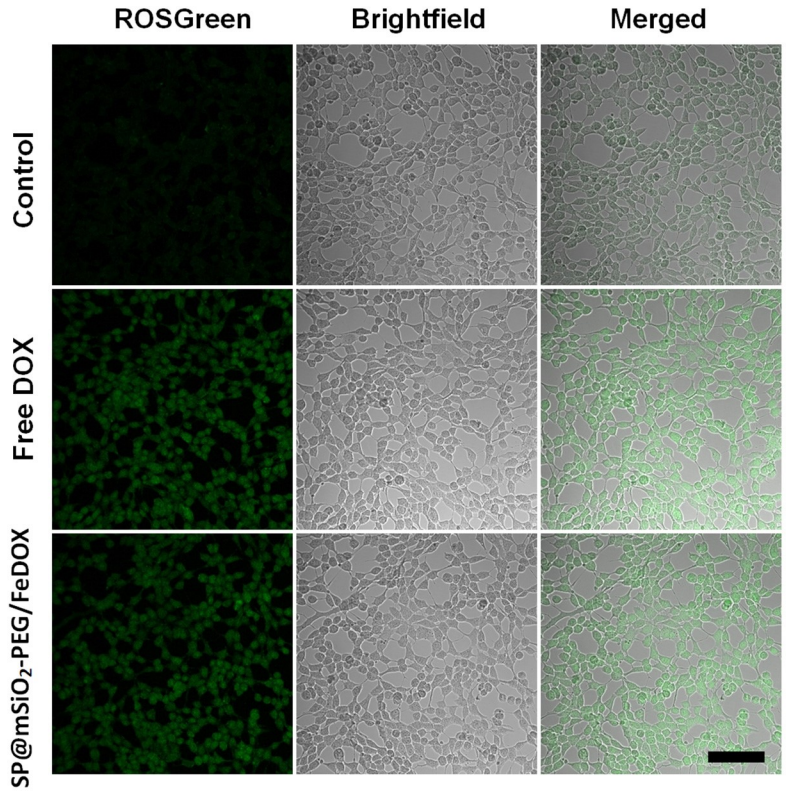

Figure S21. Intracellular H_2O_2 detection using ROSGreen as H_2O_2 probe after the treatment with DOX and SP@mSiO_2-PEG/FeDOX nanoparticles for 12 h. The scale bar is 100 μm.

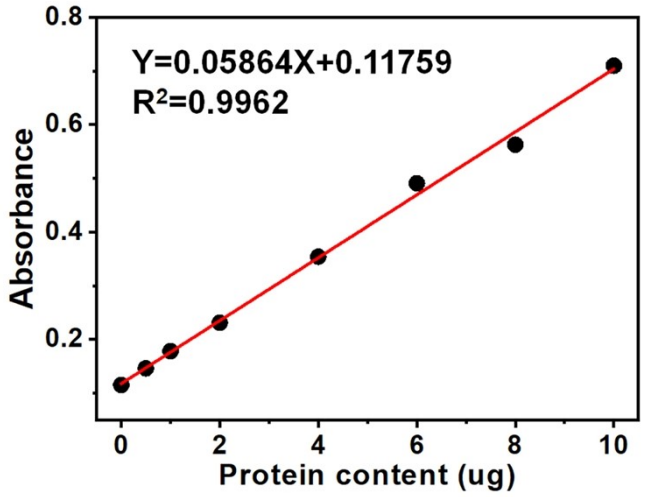

Figure S22. The working curve of the protein content in cancer cells.

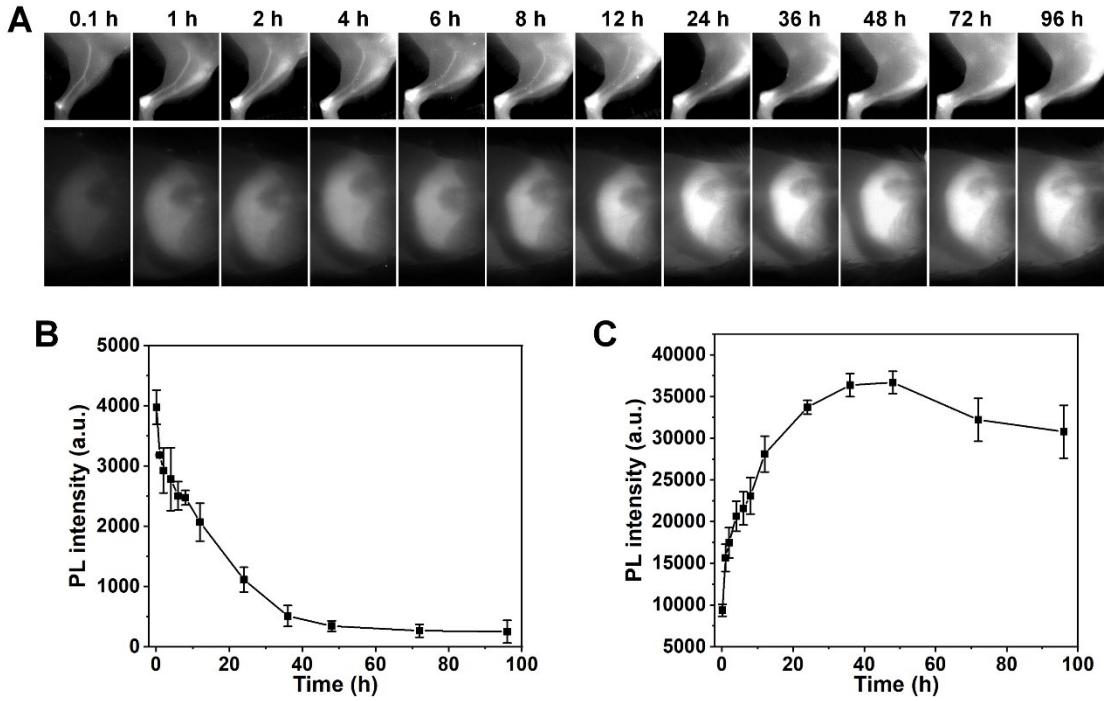

Figure S23. (A) NIR-II fluorescence images of the blood vessel and liver after injection of SP@mSiO$_2$-PEG NPs. NIR-II fluorescence intensities of the B) blood vessel and C) liver at different post-injection time.

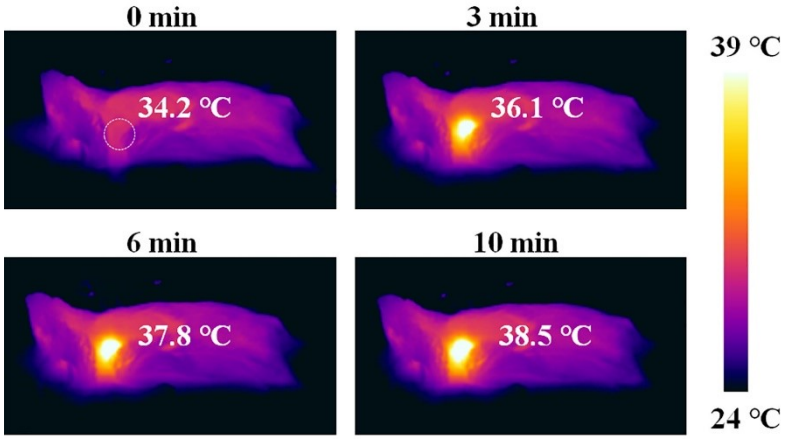

Figure S24. IR thermography of the mice during phototherapy.

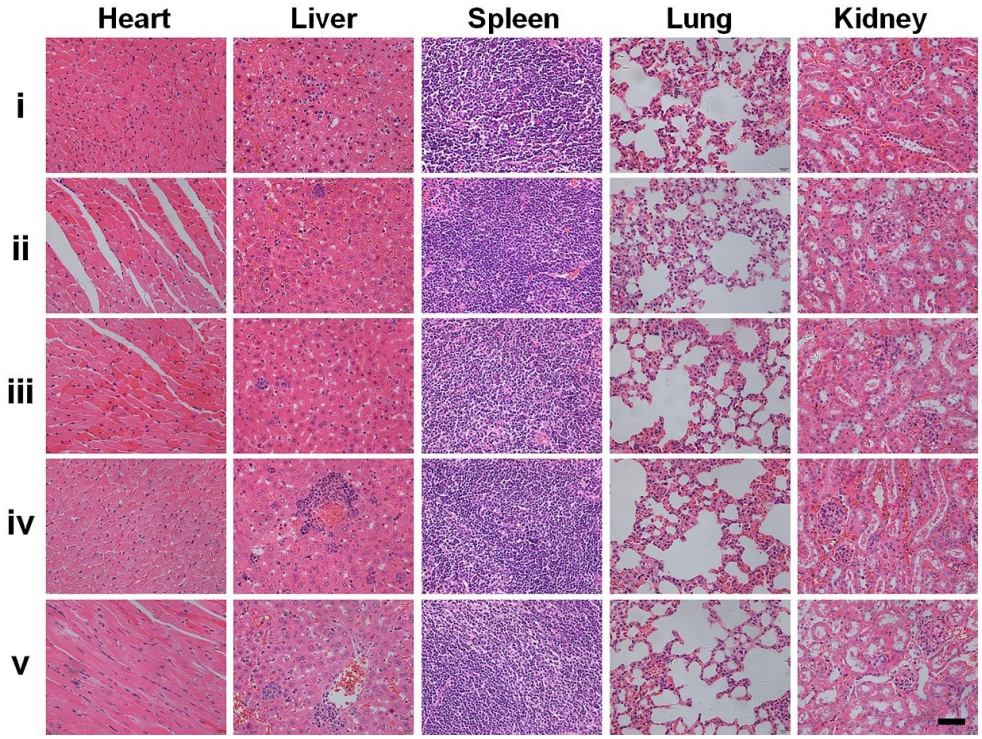

Figure S25. H&E staining of the major organs after different treatments: (i) saline, (ii) SP@mSiO$_2$-PEG, (iii) SP@mSiO$_2$-PEG/FeDOX, (iv) SP@mSiO$_2$-PEG + laser, and (v) SP@mSiO$_2$-PEG/FeDOX + laser. Scale bar: 50 μm.

References

[1] S. Albrecht, S. Janietz, W. Schindler, J. Frisch, J. Kurpiers, J. Kniepert, S. Inal, P. Pingel, K. Fostiropoulos, N. Koch, D. Neher, *J. Am. Chem. Soc.* **2012**, 134, 14932.

[2] C. J. Zhang, S. T. Lu, K. Deng, W. Qian, Y. Liu, Y. Li, S. Q. Jin, R. Y. Suo, H. B. Xu, B. Wu, *Adv. Funct. Mater.* **2023**, 33, 2301462.

[3] Y. J. Sang, F. F. Cao, W. Li, L. Zhang, Y. W. You, Q. Q. Deng, K. Dong, J. S. Ren, X. G. Qu, *J. Am. Chem. Soc.* **2020**, 142, 5177.

[4] J. Sun, X. T. Cai, C. J. Wang, K. Du, W. J. Chen, F. D. Feng, S. Wang, *J. Am. Chem. Soc.* **2021**, 143, 868.

[5] Y. A. Duan, Y. Geng, H. B. Li, G. C. Yang, S. X. Wu, L. Z. Hao, Y. Liao, Z. M. Su, *Chem. J. Chinese U.* **2011**, 32, 920.

[6] F. Lu, T. Zhao, X. J. Sun, Z. Q. Wang, Q. L. Fan, W. Huang, *Chem. Res. Chin.*

Univ. **2021**, 37, 943.

[7] F. Lu, L. Yang, Y. J. Ding, J. J. Zhu, *Adv. Funct. Mater.* **2016**, 26, 4778.

[8] Wen. Qian, *Degree Thesis*, Nanjing University of Posts & Telecommunications, December, **2019**.